3-2018

Functionalized graphene oxide as reinforcement in epoxy based nanocomposites

F. V. Ferreira

F. S. Brito

W. Franceschi

E. A. N. Simonetti

L. .S Cividanes

See next page for additional authors

Authors

F. V. Ferreira, F. S. Brito, W. Franceschi, E. A. N. Simonetti, L. .S Cividanes, Mircea Chipara, and Karen Lozano

Version of Record: https://www.sciencedirect.com/science/article/pii/S2468023017301578
Manuscript_da4c6eb45a8c15f538dd1b5ccc588af1

Functionalized graphene oxide as reinforcement in epoxy based nanocomposites

F.V. Ferreira[a,b*], F.S. Brito[a], W. Franceschi[a], E.A.N.Simonetti[c], L.S. Cividanes[a], M. Chipara[d], K. Lozano[b]

a. Department of Aeronautical and Mechanical Engineering, Technological Institute of Aeronautics (ITA), São José dos Campos-SP, Brazil. **b.** Department of Mechanical Engineering, University of Texas – Rio Grande Valley (UTRGV) – Edinburg - TX - United States. **c**. Instituto Federal de São Paulo, São José dos Campos-SP, Brazil. **d.** Department of Physics and Geology, University of Texas – Rio Grande Valley (UTRGV) – Edinburg - TX - United States

***Author for correspondence:** Filipe Vargas Ferreira | Instituto Tecnológico de Aeronáutica | Praça Marechal Eduardo Gomes, 50, Vila das Acácias CEP 12228-900, São José dos Campos, SP. Tel.: +55 12 39475958| Email: filipevargasf@gmail.com

ABSTRACT

The effects of amine-modified graphene oxide on dispersion and micro-hardness of epoxy based nanocomposites are reported. Graphene oxide was prepared by the modified Hummers method followed by hexamethylenediamine functionalization. Analysis conducted through Fourier transform infrared spectroscopy, Raman spectroscopy, X-ray photoelectron spectroscopy and atomic force microscopy-based infrared spectroscopy show that the functionalization process effectively promoted a replacement of oxygen with amine groups while simultaneously creating defects in the graphitic structure. An increase in hardness was observed for the developed nanocomposites.

Keywords: Graphene oxide; surface modification; polymer nanocomposites; mechanical properties.

1 Introduction

Graphene oxide (GO) is an important carbon-based nanomaterial and it has attracted a great interest from researchers due to its unique properties; high surface area (~2630 m^2 g^{-1}) [1], high intrinsic mobility that can reach up to 200,000 cm^2 V^{-1} s^{-1} [2], high Young modulus (~1 TPa) [3], high mechanical stiffness (>1000 GPa) [4], and exceptionally high thermal conductivity [5]. These properties make GO a very attractive material to be used as nanofiller in polymer matrices leading to the development of a new class of nanocomposites [6–8]. These composite materials have attracted extensive attention due to observed enhancements in mechanical, thermo-physical and electrical properties resulting in a variety of promising applications [9–11]. In this context, as reported by Huang et al. [12], the reinforcement efficiency of the graphene oxide in the polymer nanocomposites is better than those of the corresponding carbon nanotubes (CNTs) or functionalized CNTs.

Graphene oxide-based composite are viable candidates for a variety of industrial applications, especially for aircraft components, in particular electronics, such as supercapacitors, transistors, etc. [13–15]. However, although graphene/polymer composites have promising applications, the agglomeration of graphene sheets due to the strong van der Waals forces among their sheets and the weak compatibility with most of polymer matrices have been fundamental roadblocks that restrict its potential as a reinforcing agent [16,17]. Surface modification of graphene by adding functional groups is an effective way to reduce the tendency to agglomerate [18]. In addition, functionalization increases the graphene compatibility with specific polymers improving the reinforcing effect [19].

Several studies have investigated the effect of carbon materials functionalization on the final properties of polymer composites [20]. Chatterjee et al. [21] observed that the fracture toughness of an epoxy increased 66% after addition of 0.1 wt.% of expanded graphene nanoplatelets modified by dodecylamine. Other researchers [22] observed an increase of 72% in Young's modulus and 143% in hardness with 0.5 wt.% of amino-modified graphene by tetraethylenepentamine. The authors attributed these results to the chemical modification of the graphene. Wan et al. [23] prepared epoxy composites filled with bisphenol-A functionalized GO (DGEBA–f–GO). They observed that the surface modification of GO with DGEBA improves the compatibility and dispersion of GO sheets in epoxy matrix, resulting in improved mechanical properties of the composites. Similar results were observed by other authors working with epoxy-based composites filled with silane functionalized GO (silane-f-GO) [24], reduced graphene oxide (TRGO) [25] and polyetheramine-functionalized graphene oxide (PEA-f-GO) [26]. Other authors [27] prepared composites chemically reduced graphene oxide (CRGO) sheets grafted with poly(methyl methacrylate) (PMMA-grafted-CRGO) by emulsion polymerization. The authors observed an efficient stress transfer in the PMMA composites filled with CRGO sheets grafted with PMMA polymer molecules. Alam et al. [28] have prepared hyper branched polyester coated multi-walled carbon nanotubes (HBPCNT) by solvent evaporation technique. HBPCNT loaded unsaturated polyester (UPR) nanosuspension has been cured and investigated with differential scanning calorimetric method. The authors observed that the HBPCNT remarkably reduces the curing temperature by 13°C during crosslinking in HBPCNT-UPR nanosuspension.

Based on the above results, the addition of hexamethylenediamine functionalized graphene (AGO) into an epoxy resin has potential to improve the mechanical properties of these nanocomposites due to amino groups introduced into the graphene sheets. These amino

groups when attached to graphene sheets may increase the crosslinking process between the AGO and the polymeric matrix. Furthermore, this group may decrease graphene agglomeration resulting in an improved dispersion and distribution of the GO sheets.

To the best of the author's knowledge, the effects of graphene oxide functionalization by hexamethylenediamine (HMDE) on the thermo-physical and mechanical properties of epoxy-based nanocomposites have not yet been reported. This study further contributes to the understanding of the relationships between surface modification of graphene and their interaction with polymer matrices. Results show improved properties in the modified graphene-based nanocomposites.

2 Material and methods

2.1 Materials

2.1.1 Matrix

Araldite GY 260 based on diglycidyl ether of bisphenol A (DGEBA) with Aradur 972 based on diaminodiphenylmethane, both manufactured by Huntsman were used as the base epoxy resin.

2.1.2 Preparation of graphene oxide (GO)

The graphene oxide (GO) used in this study was prepared by a modified Hummers method [29]. An amount of 1.5 g of graphite powder was added to 120 mL of concentrated sulfuric acid (H_2SO_4, Merck, 98%) and the mixture was maintained at room temperature for 24 h. These followed by addition of 0.7 g of $NaNO_3$ (Synth, 99%), the mixture was maintained under magnetic stirring at 30^{o}C for 2 hours. After stirring, the temperature was decreased to 0ºC and 7 g of $KMnO_4$ (Synth, 90%) were added. The mixture was magnetically stirred for 2 hours. After that, 150 mL of deionized water was added and temperature was increased to 25^{o}C. The reaction was terminated by slowly adding 5 mL of H_2O_2 (Synth, 30%). The

resulting mixture was vacuum filtered and washed with deionized water until the filtered water reached a neutral pH. Finally, the graphene oxide was dried in a vacuum oven at 40ºC for 16 h.

2.1.3 Synthesis of functionalized graphene oxide by hexamethylenediamine (AGO)

The GO (0.3 g) was added to 150 mL of hexamethylenediamine (HMDA, $NH_2(CH_2)_6NH_2$, Aldrich, 70%). The mixture was maintained under magnetic stirring and heated at 100ºC for 4 days. The hexamethylenediamine functionalized graphene (AGO) was filtered using a polytetrafluorethylene (PTFE) membrane (0.45 μm pore size) and the excess HMDA was removed by washing with ethanol (Neon, 95%). After that, the AGO was dried in a vacuum oven at 40ºC for 16 h. Figure 1 shows an schematic preparation of the graphene oxide and its surface modification.

2.1.4 Preparation of Nanocomposites

The neat resin (epoxy) and composites (GO/epoxy and AGO/epoxy) were synthesized using a resin of diglycidyl ether of bisphenol A (DGEBA-3) and diaminodiphenylmethane (DDM). 1 wt% of GO and AGO were dispersed in acetone for 10 minutes in ultrasound baths. The acetone was chosen as pre-dispersing solvent because both GO and AGO showed good dispersion in acetone. Other authors reported that the use of pre-dispersing solvent helps in the preparation of nanocomposites with stronger interfacial interactions among filler and polymer matrix [30]. Then, the graphene/acetone mixture was added to the resin and mixed using tip sonication (UP 200S, Hielscher, 200 W) at 65ºC. The mixture was degassed under vacuum at 80ºC for 24 hours. The mixture was then heated to 90ºC and the curing agent was added with a resin-to-curing agent weight ratio of 100:27.

2.2 Characterization and measurements

2.2.1 Fourier transform infrared (FT-IR) spectra

FT-IR analysis was conducted in a FT-IR Spectrum One Perkin Elmer spectrometer (resolution 4 cm^{-1}, 40 scans) using the KBr pellet technique (0.2:400 mg), in the range of 4000-400 cm^{-1}.

2.2.2 Raman spectroscopy

The structural characteristics of the GO and AGO were investigated by Raman spectroscopy on a Renishaw 2000 Micro-Raman equipped with an argon laser (514.5 nm), in the range of 1000-2000 cm^{-1}.

2.2.3 X-ray photoelectron spectroscopy (XPS)

XPS analysis of the samples was performed on a commercial spectrometer (UNI-SPECS UHV), with Mg Kα line (hν =1253.6 eV) and a pass energy set at 10 eV. The composition of the surface layer was determined from the ratio of the relative peak areas corrected by Scofield sensitivity factors of the corresponding elements. The width at half maximum (FWHM) varied between 1.2 and 2.1 eV and the accuracy of the peak positions was $\pm$ 0.1.

2.2.4 Atomic Force Microscopy-based infrared spectroscopy (AFM-IR)

Nanoscale infrared analysis (AFM-IR) was performed on a NanoIR2s Anasys Instrument. The samples were subjected to pulses at a repetition rate of 180 kHz from a tunable infrared source (Quantum Cascade Lasers - Daylight) with an 1800–1600 cm^{-1} spectral range. All AFM topographic images were obtained in contact mode with resonance frequency of 13 ± 4 kHz and a spring constant of 0.07–0.4 N/m.

2.2.5 X-ray diffraction (XRD)

X-ray diffraction patterns were recorded on a high resolution X-ray diffractometer (Philips X'Pert), equipped with CuKα radiation tube, at 45 kV and 25 mA, with 2θ scans ranging from $3^o \leq 2\theta \leq 90^o$, and a scan rate of 0.42 ^{o}/s. The distance layer ($d_{(002)}$) of the samples GO and AGO was calculated based on Bragg's law (equation 1) [31].

$$\lambda = 2d_{(002)} \sin\theta \qquad (1)$$

where λ is the wavelength of the X-ray, θ is the scattering angle, d is the interplane distance of the lattices. The crystallite size (D) of the samples was determined using the Scherrer equation (equation 2):

$$D = \frac{0.9\lambda}{\delta \cos\theta} \qquad (2)$$

where δ is the integral full widths at half maximum in radians.

2.2.6 Scanning electron microscope (SEM)

SEM images were obtained using a field emission gun-scanning electron microscope (Tescan VEGA3 XMU). The samples were fixed in the sample holder with the aid of conductive carbon tape.

2.2.7 Dynamic mechanical analyses (DMA)

Dynamic mechanical analysis measurements were carried out using a DMA Q 800 (TA Instrumental Company) with a constant frequency of 1 Hz, a temperature range between 30 and 220 ^{o}C, and a heating rate of 3 ^{o}C/min. The sample dimensions were 60 x 12 x 3 mm^3. At least three samples of each composition were tested to ensure data reproducibility.

2.2.8 Hardness test

Hardness was measured with 1.96 N of load applied for 10 s using a Diamond Vickers indenter Tester FM-700. Thirty two indents were made on each surface (keeping the appropriate distance from sample edges and between indentation marks) to ensure data consistency. The hardness value HV (in GPa) was calculated from the indentation load and the diagonal of the Vickers imprint. The HV data set was analyzed using the statistical computational and graphical environment program, R with a 95% confidence interval.

3 Results and discussion

3.1 Fourier transform infrared (FT-IR) spectra

FT-IR was conducted to analyze the surface functionalization of the samples graphite, GO and AGO. The graphite spectrum (Figure 2a) showed a strong band at 3400 cm^{-1}, and double bands at 2924 and 2861 cm^{-1}, assigned to hydroxyl (ν OH) stretching vibration [32], and asymmetric (νa CH_2) and symmetric (νs CH_2) stretching vibrations of methylene group, respectively [33–35]. The spectrum also showed a band at 1639 cm^{-1}, attributed to C=C stretching [36,37]. The spectrum of the GO sample (Figure 2b) showed the appearance of a band at 1730 cm^{-1}, which is due to the carbonyl (C=O) stretch of the carboxylic acid group [38–40]. Additionally, bands at approximately 1222 and 1049 cm^{-1} were observed in the spectrum, corresponding to epoxy (C-O) stretching and the alkoxy (C-O) stretching [41,42]. After surface modification by hexamethylenediamine (Figure 2c), the bands at 1730 and 1222 cm^{-1} almost disappeared and a new band at 1570 cm^{-1} appeared, which may be related to the N-H bending stretching [41]. Further confirmation of the functionalization process are the bands appearing at 3425 and 1116 cm^{-1} attributed to the NH_2 stretch of the amine group overlapped with O-H stretching and C-N stretching vibrations, respectively [41,43]. The assignments of the infrared peaks are summarized in Table 1. These results suggest that the amine group was attached to GO surface.

3.2 Raman spectroscopy

Raman spectroscopy (Figure 3) was used to characterize the crystalline structural changes after surface modification. Raman spectrum of graphite-like materials exhibits two strong bands at D (∼1352cm^{-1}) and G (∼1590cm^{-1}). D band is associated to the disordered graphite structure (sp^3 diamond-like carbons), while G band is related to concentric cylinders of the graphene layers (C-C sp^2) [44]. Generally, the increase of the ratio of the intensities of the D

and G bands (ID/IG) indicates a decrease in the average size of the C-C sp^2 [45]. The results showed that the ID/IG value increased from 0.86 to 0.89 after surface modification, indicating a decrease in the average size of the sp^2 carbon domains (loss of aromaticity). Moreover, an increasing of full width at half maximum (FWHM) in the G band was observed confirming a loss of aromaticity after the modification process. Surface modifications involving a strong oxidant have a significant effect on the aromaticity of the carbon materials, resulting in loss of aromaticity. During the functionalization, the unsaturated π-bonds in the GO structure are destroyed by covalent linkage of functional groups and therefore topological defects and vacancies are created [46,47]. These vacancies are assigned to 5-7-7-5 rings (called Stone-Wales defects) and 5-8-5 defects, composed of two pentagonal rings and one octagonal ring [44,48]. Other authors studying covalent functionalization of graphene oxide [49], carbon nanotube [50], and carbon black [51] have also observed a loss of aromaticity after surface modification. Thus, the Raman results indicate that functionalization of GO with HMDE induces some defects in the GO surface, changing the sp^2 hybridized C-C bond to a sp^3 hybridized C-C bond.

3.3 X-ray photoelectron spectroscopy (XPS)

XPS analysis was employed in order to quantitatively identify the surface chemistry of GO and AGO (Figure 4a). The GO contains 69.1 atom% of carbon and 28.5 atom% of oxygen. After surface modification by hexamethylenediamine, the carbon content increased up to 76.0 atom%, while oxygen content decreased to 11.7 atom% (O/C ratio of 0.41 for GO and 0.15 for AGO). Additionally, the survey spectrum of AGO shows 10.4 atom% of nitrogen, which is due to the HMDA functional group attached to the graphene oxide surface (N/C ratio of 0.01 for GO and 0.14 for AGO). The C1s peaks were deconvoluted to effectively reveal the functionalization process (Figure 4b), peaks corresponding to graphitic C-C (~284.5 eV), C-H (~285.2 eV), C-N (285.8 eV), C-O epoxy group (~286.6 eV), C=O (~287.8 eV), and O-C=O

(289.5 eV) were observed [52,53]. Results of high resolution XPS spectra analyses for C1s are summarized in Table 2. A comparison of the C1s spectrum of the GO to the C1s spectrum of the AGO showed a decrease for the C-C sp^2, indicating a loss of aromaticity after surface modification. The functionalization using strong oxidants induces some defects in the GO surface, as observed in Raman spectroscopy. Simultaneously, the peaks assigned to oxygenated carbon (C-O, C=O, O-C=O) decreased and a new peak at 285.8 eV assigned to nitrogenated functional group appeared, suggesting that the amine group was covalently linked to the AGO surface by replacement of oxygen of the oxygenated carbons. The XPS results are in agreement with the FT-IR and Raman analysis, all depict that HMDA has been successfully grafted onto GO surface via covalent bonds.

3.4 Morphological investigation

SEM micrographs (Figure 5) were taken from the GO and AGO to investigate the integrity of the graphene oxide after surface modification. GO shows a thin rippled morphology similar to a tissue paper. After functionalization, more irregular and rough texture was observed, which can be indicative of structural defects on the AGO surface. As discussed earlier, the small increase of the ID/IG intensity observed in the Raman spectra is related to topological defects and vacancies. This interpretation can be confirmed by SEM.

3.5 Atomic Force Microscopy-based infrared spectroscopy (AFM-IR)

AFM-IR spectroscopy is a new and powerful way to characterize surface modification of nanomaterials due to a combination of the spatial resolution of AFM with the chemical analysis capability of spectroscopy [54]. This method consists of detecting the local thermal expansion of the absorbing region of the sample in response to infrared excitation [55]. In our study, the IR laser was tuned to a wavelength at 1730 cm^{-1} (corresponding to the stretch of the carboxylic acid group). Thus, the samples with a higher concentration of carboxylic acid

groups absorb light at this wavenumber and the thermal expansion of the absorbing region is identified. Figure 6a and Figure 6b show the folded and/or overlapped nanosheets of GO and AGO, respectively. The chemical image simultaneously obtained at 1730 cm^{-1} is showed in Figure 6c and Figure 6d. The blue region indicates low infrared absorptivity, while yellow and pink indicate areas of greater absorptivity. Only the GO sample shows a distinct absorption at 1730 cm^{-1}. Since this band is related to C=O (1730 cm^{-1}) and the thermal expansion signal detected in AFM-IR is in proportion to the sample absorption, it is fair to consider that the AGO has fewer C=O groups than GO. The decrease of the intensity of this band can be attributed to an amine group covalently linked to the surface of the graphene oxide through the reaction with the carboxylic acid group. It is important to note that the AFM-IR technique presents a limited performance given that the N-H bending stretching of the HMDA group occurs at 1570 cm^{-1} and the amplitude was recorded at a wavenumber range of 1800-1600 cm^{-1}. Despite this, the AFM-IR results showed good correlation with FT-IR and XPS results and confirm the surface modification of the GO.

3.6 X-ray diffraction (XRD)

The XRD patterns of graphite, GO and AGO are shown in Figure 7. The graphite sample (Figure 7a) shows a sharp peak at $2\theta = 26.7^{o}$ assigned to the diffraction of the (002) plane of the well-ordered graphene [56,57]. Graphene oxide (Figure 7b) exhibits a strong peak at $2\theta = 10.1^{o}$ (002), which may be attributable to an increase in the interlayer spacing (from 0.34 to 0.87 nm) due to oxygen-containing functional groups on the graphene oxide surface [41,56]. After functionalization with the amine groups (Figure 7c), the typical sharp peak of graphene oxide at $2\theta = 10.1^{o}$ disappeared and a broad peak at $2\theta = 22.1\ ^{o}$ (002) appeared, suggesting that graphene oxide was reduced to graphene and the interlayer spacing of graphene sheets was decreased (0.40 nm) due to a decrease of oxygenated carbon [57,58]. Moreover, the crystallite size of the samples decreased after surface modification from 11.0 to

1.4 as result of loss of aromaticity due to functionalization process (as previously discussed). This means that the GO was reduced to graphene.

3.7 Analysis of nanocomposites

Samples from the neat epoxy, GO/epoxy and AGO/epoxy composites were cryogenically fractured to be analyzed under scanning electron microscopy. Neat epoxy (Figure 8a-b) shows a flat and smooth surface, while composites presented rough and rugged surface. The nanocomposite containing GO (Figure 8c-d) exhibited large agglomerates due to the Van der Waals interaction between the planar structures of the graphene [16]. These agglomerates weaken the composite, decreasing the mechanical performance of the polymer [59,60]. On the other hand, AGO shows better homogeneity within the polymeric matrix, the fracture surface was homogeneously coated by epoxy (Fig. 8e-f), indicating that AGO was effectively dispersed. This can be attributed to the existence of amine groups on the surface of graphene oxide. Addition of the amine groups on the graphene oxide prevents agglomeration due to steric factors while can effectively promoting interactions (anchor points) between the modified graphene and the polymeric matrix through crosslinking process [16].

3.8. Dynamic mechanical analyses (DMA)

Dynamic mechanical analysis (DMA) was performed in order to assess the information on the viscoelastic properties of the composites. The variation of the storage modulus (E') and the damping factor (tanδ) of the samples are presented in Figure 9 and the values of storage modulus, tanδ, and glass transition temperature (T_g) are summarized in Table 3. The nanocomposites exhibited higher storage modulus than neat resin, given the reinforcing effect of graphene on the matrix (Figure 9a). Additionally, small differences are observed in the values of storage moduli for GO/epoxy and AGO/epoxy. The addition of graphene (modified or not) to polymer matrix leads to a phase formation at interface between filler-matrix which

contributes to dissipate energy from external stresses by frictions between particle-particle and particle-polymer at interface [61–63]. Tanδ is a measure of the damping properties of materials and can be determined by the ratio between the loss modulus and the storage modulus [64,65]. Tanδ value of nanocomposites GO/epoxy decreased slightly when compared to the neat epoxy, and the lowest value for the tanδ was for the AGO loaded epoxy system. This behavior probably occurs because the addition of fillers affects the damping behavior of the polymer owing to stress concentrations [66]. Additionally, a good adhesion between graphene and epoxy resin limits the mobility of the polymer chains reducing the values of tanδ [64,67]. T_g shifts to a lower temperature range when the composites are compared with pure epoxy (Figure 9b). The reduction in the T_g may be attributed to the enlarged free volume between the epoxy chains due to the introduction of the nanofiller into the polymer [58].

3.8 Hardness test

Figure 10 shows the results obtained from Vickers hardness testing. The hardness increased from 17.1 to 19.0 HV after adding of GO in epoxy resin whereas for the AGO composites the Vickers hardness increased to 25.3 HV, about 33% higher than the GO based composites and about 48% higher than the neat epoxy. The increase of hardness observed in the AGO/epoxy suggests that amino groups attached on graphene oxide surface decreased the strong self-interaction of graphene sheets (as observed in SEM images) therefore promoting better dispersion and more homogenous distribution of forces throughout the carbon structure and epoxy matrix. Furthermore, the amino groups served as anchor points for polymer chains, increasing the interaction between filler and matrix. The addition of graphene with uniform dispersion and strong interaction promotes a more effective dissipation of energy from external stresses. Similar improvements on hardness were observed in other studies working epoxy based composites reinforced with carbon nanotubes functionalized with

hexamethylenediamine [68], graphene nanoplatelets modified by dodecylamine [21] and amino-modified graphene by tetraethylenepentamine [22].

4 Conclusions

This study reported the functionalization of graphene oxide and its effect on the mechanical properties of epoxy based composites. The results provide evidence that GO was effectively functionalized by HMDE through replacement of oxygen groups. The functionalization process also generated defects in the graphitic structure of the samples. Surface modification improves the dispersion and interaction between modified graphene oxide and the selected epoxy resin. Hardness testing showed a 33% increase for the AGO reinforced epoxy composites when compared to the GO reinforced epoxy composites. The surface modification presented in this study shows to be an efficient method for the production of high performance graphene-based nanocomposites.

Acknowledgements

The authors would like to express their gratitude for the assistance of Evandro Lanzoni from LNNano/CNPEM with AFM-IR spectroscopy. The authors acknowledge FAPESP (Grants 2013/20218-0 and 2014/17492-6) and CNPq (Grant 141197/2014-5) for financial support, and LNNano/CNPEM and LEFE/UNESP for collaboration. We also gratefully acknowledge support received by NSF PREM award under grant No. DMR-1523577:UTRGV-UMN Partnership for Fostering Innovation by Bridging Excellence in Research and Student Success.

REFERENCES

[1] M.J. McAllister, J.-L. Li, D.H. Adamson, H.C. Schniepp, A.A. Abdala, J. Liu, M. Herrera-Alonso, D.L. Milius, R. Car, R.K. Prud'homme, I.A. Aksay, Single Sheet Functionalized Graphene by Oxidation and Thermal Expansion of Graphite, Chem. Mater. 19 (2007) 4396–4404. doi:10.1021/cm0630800.

[2] F.V. Ferreira, L.S. Cividanes, F.S. Brito, B.R.C. de Menezes, W. Franceschi, E.A.N. Simonetti, G.P. Thim, Functionalizing of Graphene and Applications: Review, 1st ed., Springer, 2016. doi:10.1007/978-3-319-35110-0_1.

[3] T. Ramanathan, A.A. Abdala, S. Stankovich, D.A. Dikin, M. Herrera-Alonso, R.D. Piner, D.H. Adamson, H.C. Schniepp, X. Chen, R.S. Ruoff, S.T. Nguyen, I.A. Aksay, R.K. Prud'Homme, L.C. Brinson, Functionalized graphene sheets for polymer nanocomposites, Nat. Nanotechnol. 3 (2008) 327–331. doi:10.1038/nnano.2008.96.

[4] R. Rohini, P. Katti, S. Bose, Tailoring the interface in graphene / thermoset polymer composites : A critical review, Polymer (Guildf). 70 (2015) A17–A34. doi:10.1016/j.polymer.2015.06.016.

[5] O.C. Compton, B. Jain, D.A. Dikin, A. Abouimrane, K. Amine, S.T. Nguyen, Chemically Active Reduced Graphene Oxide with Tunable C/O Ratios, ACS Nano. 5 (2011) 4380–4391. doi:10.1021/nn1030725.

[6] W.-W. Liu, S.-P. Chai, A.R. Mohamed, U. Hashim, Synthesis and characterization of graphene and carbon nanotubes: A review on the past and recent developments, J. Ind. Eng. Chem. 20 (2014) 1171–1185. doi:10.1016/j.jiec.2013.08.028.

[7] S.I. Abdullah, M.N.M. Ansari, Mechanical properties of graphene oxide (GO)/epoxy composites, HBRC J. 11 (2015) 151–156. doi:10.1016/j.hbrcj.2014.06.001.

[8] Y. Zhong, Z. Zhen, H. Zhu, Graphene: fundamental research and potential applications, FlatChem. (2017). doi:10.1016/j.flatc.2017.06.008.

[9] Q. Zhang, Z. Wu, N. Li, Y. Pu, B. Wang, T. Zhang, J. Tao, Advanced review of graphene-based nanomaterials in drug delivery systems: Synthesis, modification, toxicity and application, Mater. Sci. Eng. C. 77 (2017) 1363–1375. doi:10.1016/j.msec.2017.03.196.

[10] M. Allen, Honeycomb carbon -- A study of graphene, Am. Chem. Soc. (2009) 184. doi:10.1021/cr900070d.

[11] C.I.L. Justino, A.R. Gomes, A.C. Freitas, A.C. Duarte, T.A.P. Rocha-Santos, Graphene based sensors and biosensors, TrAC Trends Anal. Chem. 91 (2017) 53–66. doi:10.1016/j.trac.2017.04.003.

[12] N.-J. Huang, J. Zang, G.-D. Zhang, L.-Z. Guan, S.-N. Li, L. Zhao, L.-C. Tang, Efficient interfacial interaction for improving mechanical properties of polydimethylsiloxane nanocomposites filled with low content of graphene oxide nanoribbons, RSC Adv. 7 (2017) 22045–22053. doi:10.1039/C7RA02439H.

[13] E. Bafekrpour, G.P. Simon, J. Habsuda, M. Naebe, C. Yang, B. Fox, Fabrication and characterization of functionally graded synthetic graphite/phenolic nanocomposites, Mater. Sci. Eng. A. 545 (2012) 123–131. doi:10.1016/j.msea.2012.02.097.

[14] D. Tang, G. Ma, L. Zhang, G. Chen, Graphene?epoxy composite electrode fabricated by in situ polycondensation for enhanced amperometric detection in capillary electrophoresis, J. Chromatogr. A. 1316 (2013) 127–134. doi:10.1016/j.chroma.2013.09.077.

[15] S. Gupta, S. Chatterjee, A.K. Ray, A.K. Chakraborty, Sensors and Actuators B : Chemical Graphene – metal oxide nanohybrids for toxic gas sensor : A review, Sensors Actuators B. Chem. 221 (2015) 1170–1181. doi:10.1016/j.snb.2015.07.070.

[16] S.H. Ryu, J.H. Sin, A.M. Shanmugharaj, Study on the effect of hexamethylene diamine functionalized graphene oxide on the curing kinetics of epoxy nanocomposites, Eur. Polym. J. 52 (2014) 88–97. doi:10.1016/j.eurpolymj.2013.12.014.

[17] R. Wang, Z. Li, W. Liu, W. Jiao, L. Hao, F. Yang, Attapulgite?graphene oxide hybrids as thermal and mechanical reinforcements for epoxy composites, Compos. Sci. Technol. 87 (2013) 29–35. doi:10.1016/j.compscitech.2013.08.002.

[18] F.V. Ferreira, L.D.S. Cividanes, F.S. Brito, B.R.C. de Menezes, W. Franceschi, E.A.N. Simonetti, G.P. Thim, Functionalization of Carbon Nanotube and Applications, in: Funct. Graphene Carbon Nanotub., Springer International Publishing, 2016: pp. 31–61. doi:10.1007/978-3-319-35110-0_2.

[19] J. Phiri, P. Gane, T.C. Maloney, General overview of graphene: Production, properties and application in polymer composites, Mater. Sci. Eng. B. 215 (2017) 9–28. doi:10.1016/j.mseb.2016.10.004.

[20] L.S. Cividanes, W. Franceschi, F.V. Ferreira, B.R.C. Menezes, R.C.M. Sales, G.P. Thim, How Do CNT affect the branch and crosslink reactions in CNT-epoxy, Mater. Res. Express. 4 (2017) 105101. doi:10.1088/2053-1591/aa8d31.

[21] S. Chatterjee, J.W. Wang, W.S. Kuo, N.H. Tai, C. Salzmann, W.L. Li, R. Hollertz, F.A. Nesch, B.T.T. Chu, Mechanical reinforcement and thermal conductivity in expanded graphene nanoplatelets reinforced epoxy composites, Chem. Phys. Lett. 531 (2012) 6–10. doi:10.1016/j.cplett.2012.02.006.

[22] H. Ribeiro, W.M. Da Silva, J.C. Neves, H.D.R. Calado, R. Paniago, L.M. Seara, D. Das Mercês Camarano, G.G. Silva, Multifunctional nanocomposites based on tetraethylenepentamine-modified graphene oxide/epoxy, Polym. Test. 43 (2015) 182–192. doi:10.1016/j.polymertesting.2015.03.010.

[23] Y.J. Wan, L.C. Tang, L.X. Gong, D. Yan, Y.B. Li, L. Bin Wu, J.X. Jiang, G.Q. Lai, Grafting of epoxy chains onto graphene oxide for epoxy composites with improved mechanical and thermal properties, Carbon N. Y. 69 (2014) 467–480. doi:10.1016/j.carbon.2013.12.050.

[24] Y.-J. Wan, L.-X. Gong, L.-C. Tang, L.-B. Wu, J.-X. Jiang, Mechanical properties of epoxy composites filled with silane-functionalized graphene oxide, Compos. Part A Appl. Sci. Manuf. 64 (2014) 79–89. doi:10.1016/j.compositesa.2014.04.023.

[25] J. Zang, Y.-J. Wan, L. Zhao, L.-C. Tang, Fracture Behaviors of TRGO-Filled Epoxy Nanocomposites with Different Dispersion/Interface Levels, Macromol. Mater. Eng. 300 (2015) 737–749. doi:10.1002/mame.201400437.

[26] L.-Z. Guan, Y.-J. Wan, L.-X. Gong, D. Yan, L.-C. Tang, L.-B. Wu, J.-X. Jiang, G.-Q. Lai, Toward effective and tunable interphases in graphene oxide/epoxy composites by grafting different chain lengths of polyetheramine onto graphene oxide, J. Mater. Chem. A. 2 (2014) 15058. doi:10.1039/C4TA02429J.

[27] L.-X. Gong, Y.-B. Pei, Q.-Y. Han, L. Zhao, L.-B. Wu, J.-X. Jiang, L.-C. Tang, Polymer grafted reduced graphene oxide sheets for improving stress transfer in polymer composites, Compos. Sci. Technol. 134 (2016) 144–152. doi:10.1016/j.compscitech.2016.08.014.

[28] A.K.M.M. Alam, M.D.H. Beg, R.M. Yunus, M.F. Mina, K.H. Maria, T. Mieno, Evolution of functionalized multi-walled carbon nanotubes by dendritic polymer coating and their anti-scavenging behavior during curing process, Mater. Lett. 167 (2016) 58–60. doi:10.1016/j.matlet.2015.12.130.

[29] W.S. Hummers, R.E. Offeman, Preparation of Graphitic Oxide, J. Am. Chem. Soc. 80 (1958) 1339–1339. doi:10.1021/ja01539a017.

[30] M.D.H. Beg, A.K.M. Moshiul Alam, R.M. Yunus, M.F. Mina, Improvement of interaction between pre-dispersed multi-walled carbon nanotubes and unsaturated polyester resin, J. Nanoparticle Res. 17 (2015) 53. doi:10.1007/s11051-014-2846-8.

[31] A.K.M.M. Alam, M.D.H. Beg, R.M. Yunus, Microstructure and fractography of multiwalled carbon nanotube reinforced unsaturated polyester nanocomposites, Polym. Compos. 38 (2017) E462–E471. doi:10.1002/pc.23911.

[32] F.V. Ferreira, L.D.S. Cividanes, F.S. Brito, B.R.C. de Menezes, W. Franceschi, E.A. Nunes Simonetti, G.P. Thim, Functionalizing Graphene and Carbon Nanotubes, Springer International Publishing, Cham, 2016. doi:10.1007/978-3-319-35110-0.

[33] G. Vukovic, A. Marinkovic, M. Obradovic, V. Radmilovic, M. ?oli?, R. Aleksi?, P.S. Uskokovi?, Synthesis, characterization and cytotoxicity of surface amino-functionalized water-dispersible multi-walled carbon nanotubes, Appl. Surf. Sci. 255 (2009) 8067–8075. doi:10.1016/j.apsusc.2009.05.016.

[34] F.V. Ferreira, W. Francisco, B.R.C. De Menezes, L.S. Cividanes, A.D.R. Coutinho, G.P. Thim, Carbon nanotube functionalized with dodecylamine for the effective dispersion in solvents, Appl. Surf. Sci. 357 (2015) 2154–2159. doi:10.1016/j.apsusc.2015.09.202.

[35] F.V. Ferreira, I.F. Pinheiro, R.F. Gouveia, G.P. Thim, L.M.F. Lona, Functionalized cellulose nanocrystals as reinforcement in biodegradable polymer nanocomposites, Polym. Compos. (2017). doi:10.1002/pc.24583.

[36] X. Li, Y. Zhao, W. Wu, J. Chen, G. Chu, H. Zou, Synthesis and characterizations of graphene–copper nanocomposites and their antifriction application, J. Ind. Eng. Chem. 20 (2014) 2043–2049. doi:10.1016/j.jiec.2013.09.029.

[37] J. Gu, X. Yang, Z. Lv, N. Li, C. Liang, Q. Zhang, Functionalized graphite nanoplatelets/epoxy resin nanocomposites with high thermal conductivity, Int. J. Heat Mass Transf. 92 (2016) 15–22. doi:10.1016/j.ijheatmasstransfer.2015.08.081.

[38] N. Liu, X. Wang, W. Xu, H. Hu, J. Liang, J. Qiu, Microwave-assisted synthesis of MoS2/graphene nanocomposites for efficient hydrodesulfurization, Fuel. 119 (2014) 163–169. doi:10.1016/j.fuel.2013.11.045.

[39] L.S. Cividanes, D.D. Brunelli, E.F. Antunes, E.J. Corat, K.K. Sakane, G.P. Thim, Cure

study of epoxy resin reinforced with multiwalled carbon nanotubes by Raman and luminescence spectroscopy, J. Appl. Polym. Sci. 127 (2013) 544–553. doi:10.1002/app.37815.

[40] I.F. Pinheiro, F.V. Ferreira, D.H.S. Souza, R.F. Gouveia, L.M.F. Lona, A.R. Morales, L.H.I. Mei, Mechanical, rheological and degradation properties of PBAT nanocomposites reinforced by functionalized cellulose nanocrystals, Eur. Polym. J. 97 (2017) 356–365. doi:10.1016/j.eurpolymj.2017.10.026.

[41] A. Yang, J. Li, C. Zhang, W. Zhang, N. Ma, One-step amine modification of graphene oxide to get a green trifunctional metal-free catalyst, Appl. Surf. Sci. 346 (2015) 443–450. doi:10.1016/j.apsusc.2015.04.033.

[42] J. Ryu, M. Han, Improvement of the mechanical and electrical properties of polyamide 6 nanocomposites by non-covalent functionalization of multi-walled carbon nanotubes, Compos. Sci. Technol. 102 (2014) 169–175. doi:10.1016/j.compscitech.2014.07.022.

[43] S.-D. Pan, L.-X. Zhou, Y.-G. Zhao, X.-H. Chen, H.-Y. Shen, M.-Q. Cai, M.-C. Jin, Amine-functional magnetic polymer modified graphene oxide as magnetic solid-phase extraction materials combined with liquid chromatography?tandem mass spectrometry for chlorophenols analysis in environmental water, J. Chromatogr. A. 1362 (2014) 34–42. doi:10.1016/j.chroma.2014.08.027.

[44] A. Maio, R. Fucarino, R. Khatibi, S. Rosselli, M. Bruno, R. Scaffaro, A novel approach to prevent graphene oxide re-aggregation during the melt compounding with polymers, Compos. Sci. Technol. 119 (2015) 131–137. doi:10.1016/j.compscitech.2015.10.006.

[45] M.S. Dresselhaus, G. Dresselhaus, R. Saito, A. Jorio, Raman spectroscopy of carbon nanotubes, Phys. Rep. 409 (2005) 47–99. doi:10.1016/j.physrep.2004.10.006.

[46] H.C. Schniepp, J.-L. Li, M.J. McAllister, H. Sai, M. Herrera-Alonso, D.H. Adamson, R.K. Prud'homme, R. Car, D.A. Saville, I.A. Aksay, Functionalized Single Graphene Sheets Derived from Splitting Graphite Oxide, J. Phys. Chem. B. 110 (2006) 8535–8539. doi:10.1021/jp060936f.

[47] G. Mittal, V. Dhand, K.Y. Rhee, S.-J. Park, W.R. Lee, A review on carbon nanotubes and graphene as fillers in reinforced polymer nanocomposites, J. Ind. Eng. Chem. 21 (2015) 11–25. doi:10.1016/j.jiec.2014.03.022.

[48] K.N. Kudin, B. Ozbas, H.C. Schniepp, R.K. Prud'homme, I.A. Aksay, R. Car, Raman Spectra of Graphite Oxide and Functionalized Graphene Sheets, Nano Lett. 8 (2008) 36–41. doi:10.1021/nl071822y.

[49] B. Xue, J. Zhu, N. Liu, Y. Li, Facile functionalization of graphene oxide with ethylenediamine as a solid base catalyst for Knoevenagel condensation reaction, Catal. Commun. 64 (2015) 105–109. doi:10.1016/j.catcom.2015.02.003.

[50] F. V. Ferreira, W. Francisco, B.R.C. Menezes, F.S. Brito, A.S. Coutinho, L.S. Cividanes, A.R. Coutinho, G.P. Thim, Correlation of surface treatment, dispersion and mechanical properties of HDPE/CNT nanocomposites, Appl. Surf. Sci. 389 (2016) 921–929. doi:10.1016/j.apsusc.2016.07.164.

[51] M.C.F. Soares, M.M. Viana, Z.L. Schaefer, V.S. Gangoli, Y. Cheng, V. Caliman, M.S. Wong, G.G. Silva, Surface modification of carbon black nanoparticles by dodecylamine: Thermal stability and phase transfer in brine medium, Carbon N. Y. 72 (2014) 287–295. doi:10.1016/j.carbon.2014.02.008.

[52] S. Park, K.-S. Lee, G. Bozoklu, W. Cai, S.T. Nguyen, R.S. Ruoff, Graphene Oxide Papers Modified by Divalent Ions?Enhancing Mechanical Properties via Chemical Cross-Linking, ACS Nano. 2 (2008) 572–578. doi:10.1021/nn700349a.

[53] D.G.D. Galpaya, J.F.S. Fernando, L. Rintoul, N. Motta, E.R. Waclawik, C. Yan, G.A. George, The effect of graphene oxide and its oxidized debris on the cure chemistry and interphase structure of epoxy nanocomposites, Polymer (Guildf). 71 (2015) 122–134. doi:10.1016/j.polymer.2015.06.054.

[54] A. Dazzi, C.B. Prater, Q. Hu, D.B. Chase, J.F. Rabolt, C. Marcott, AFM-IR: Combining Atomic Force Microscopy and Infrared Spectroscopy for Nanoscale Chemical Characterization, Appl. Spectrosc. 66 (2012) 1365–1384. doi:10.1366/12-06804.

[55] A. Dazzi, C.B. Prater, AFM-IR: Technology and Applications in Nanoscale Infrared Spectroscopy and Chemical Imaging, Chem. Rev. (2016) acs.chemrev.6b00448. doi:10.1021/acs.chemrev.6b00448.

[56] A. Ashori, H. Rahmani, R. Bahrami, Preparation and characterization of functionalized graphene oxide/carbon fiber/epoxy nanocomposites, Polym. Test. 48 (2015) 82–88. doi:10.1016/j.polymertesting.2015.09.010.

[57] A.M. Shanmugharaj, J.H. Yoon, W.J. Yang, S.H. Ryu, Synthesis, characterization, and surface wettability properties of amine functionalized graphene oxide films with varying amine chain lengths, J. Colloid Interface Sci. 401 (2013) 148–154. doi:10.1016/j.jcis.2013.02.054.

[58] X. Zhang, O. Alloul, Q. He, J. Zhu, M.J. Verde, Y. Li, S. Wei, Z. Guo, Strengthened magnetic epoxy nanocomposites with protruding nanoparticles on?the graphene nanosheets, Polymer (Guildf). 54 (2013) 3594–3604. doi:10.1016/j.polymer.2013.04.062.

[59] F.V. Ferreira, W. Franceschi, B.R.C. Menezes, F.S. Brito, K. Lozano, A.R. Coutinho, L.S. Cividanes, G.P. Thim, Dodecylamine functionalization of carbon nanotubes to improve dispersion, thermal and mechanical properties of polyethylene based nanocomposites, Appl. Surf. Sci. 410 (2017) 267–277. doi:10.1016/j.apsusc.2017.03.098.

[60] S.L. Ruan, P. Gao, X.G. Yang, T.X. Yu, Toughening high performance ultrahigh molecular weight polyethylene using multiwalled carbon nanotubes, Polymer (Guildf). 44 (2003) 5643–5654. doi:10.1016/S0032-3861(03)00628-1.

[61] Y. Huang, S. Jiang, L. Wu, Y. Hua, Characterization of LLDPE/nano-SiO2 composites by solid-state dynamic mechanical spectroscopy, Polym. Test. 23 (2004) 9–15. doi:10.1016/S0142-9418(03)00048-5.

[62] F. V. Ferreira, B.R.C. Menezes, W. Franceschi, E. V. Ferreira, K. Lozano, L.S.

Cividanes, A.R. Coutinho, G.P. Thim, Influence of carbon nanotube concentration and sonication temperature on mechanical properties of HDPE/CNT nanocomposites, Fullerenes, Nanotub. Carbon Nanostructures. 25 (2017) 531–539. doi:10.1080/1536383X.2017.1359553.

[63] F. V. Ferreira, L.S. Cividanes, R.F. Gouveia, L.M.F. Lona, An overview on properties and applications of poly(butylene adipate- co -terephthalate)-PBAT based composites, Polym. Eng. Sci. (2017). doi:10.1002/pen.24770.

[64] V. Fiore, T. Scalici, G. Vitale, A. Valenza, Static and dynamic mechanical properties of Arundo Donax fillers-epoxy composites, Mater. Des. 57 (2014) 456–464. doi:10.1016/j.matdes.2014.01.025.

[65] M.M. Rahman, M. Hosur, A.G. Ludwick, S. Zainuddin, A. Kumar, J. Trovillion, S. Jeelani, Thermo-mechanical behavior of epoxy composites modified with reactive polyol diluent and randomly-oriented amino-functionalized multi-walled carbon nanotubes, Polym. Test. 31 (2012) 777–784. doi:10.1016/j.polymertesting.2012.05.006.

[66] D. Shanmugam, M. Thiruchitrambalam, Static and dynamic mechanical properties of alkali treated unidirectional continuous Palmyra Palm Leaf Stalk Fiber/jute fiber reinforced hybrid polyester composites, Mater. Des. 50 (2013) 533–542. doi:10.1016/j.matdes.2013.03.048.

[67] A.L. Martenez-Hern?ndez, C. Velasco-Santos, M. De-Icaza, V.M. Casta?o, Dynamical-mechanical and thermal analysis of polymeric composites reinforced with keratin biofibers from chicken feathers, Compos. Part B Eng. 38 (2007) 405–410. doi:10.1016/j.compositesb.2006.06.013.

[68] W. Francisco, F.V. Ferreira, E.V. Ferreira, L.S. Cividanes, A. dos R. Coutinho, G.P. Thim, Functionalization of multi-walled carbon nanotube and mechanical property of epoxy-based nanocomposite, J. Aerosp. Technol. Manag. 7 (2015) 289–293. doi:10.5028/jatm.v7i3.485.

Figures

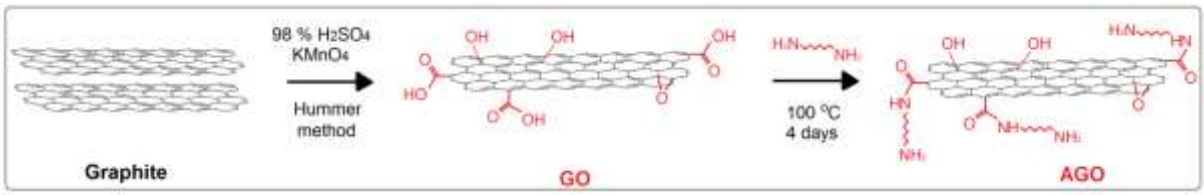

Figure 1 - Schematic of the preparation of graphene oxide by the Hummers method (GO) and surface modification using hexamethylenediamine (AGO).

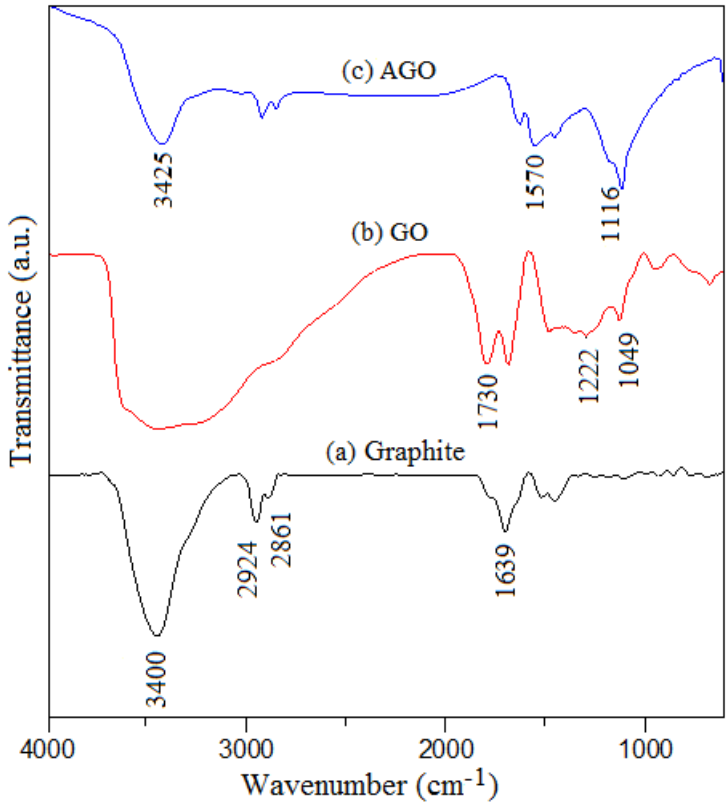

Figure 2 - FTIR transmission spectra of (a) graphite, (b) GO and (c) AGO.

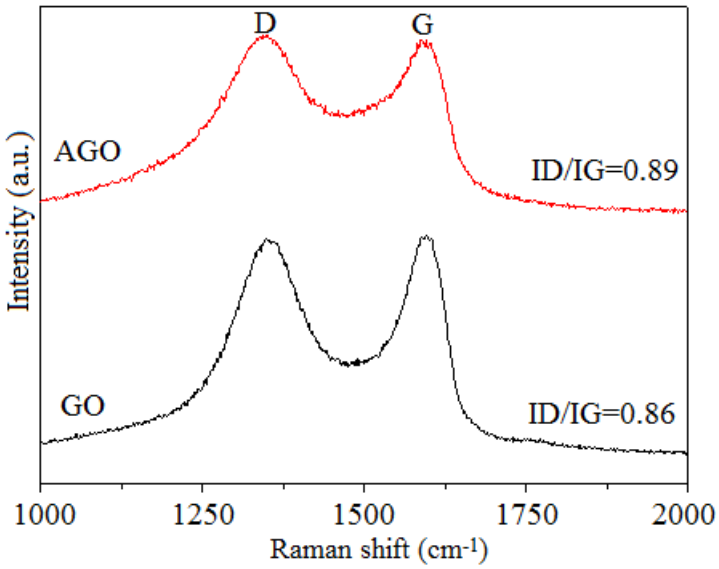

Figure 3 - Raman spectra of GO and AGO.

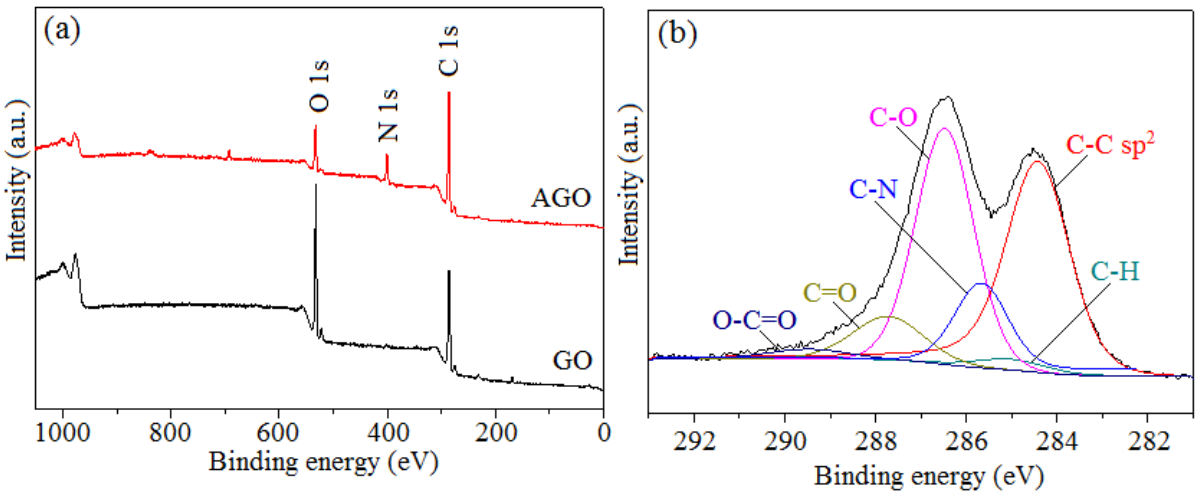

Figure 4 - (a) XPS survey spectra of GO and AGO. (b) Deconvoluted peaks of C1s XPS spectrum.

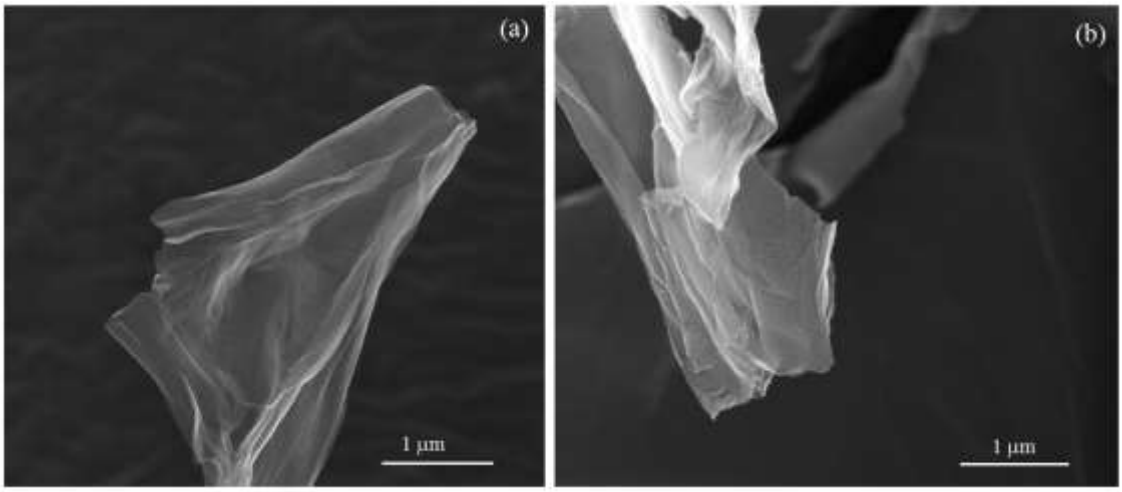

Figure 5 - Typical SEM micrographs of (a) GO and (b) AGO.

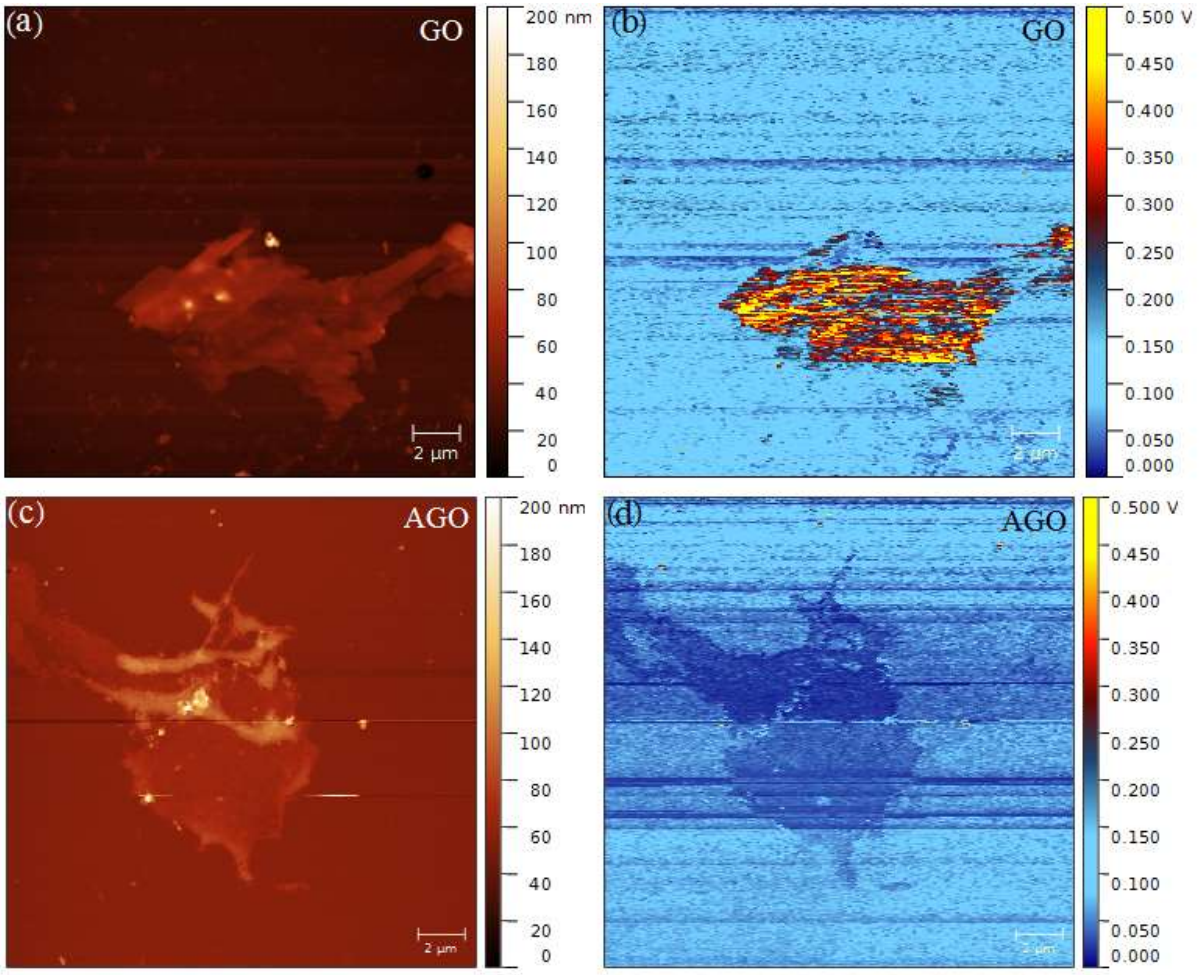

Figure 6 - Height mode AFM images (a and c) and chemical images (b and d) simultaneously obtained at 1730 cm^{-1} for the GO and AGO samples.

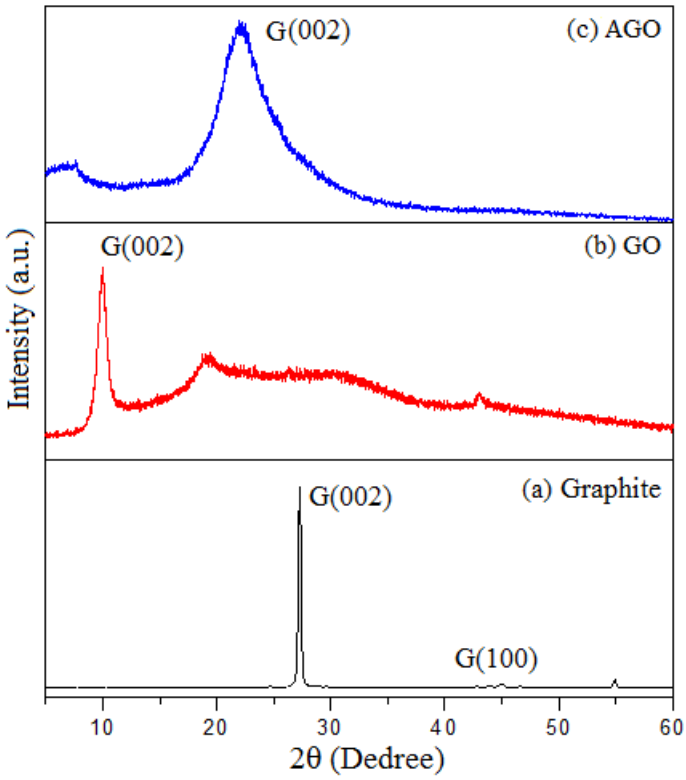

Figure 7 - XRD patterns of (a) graphite, (b) GO and (c) AGO.

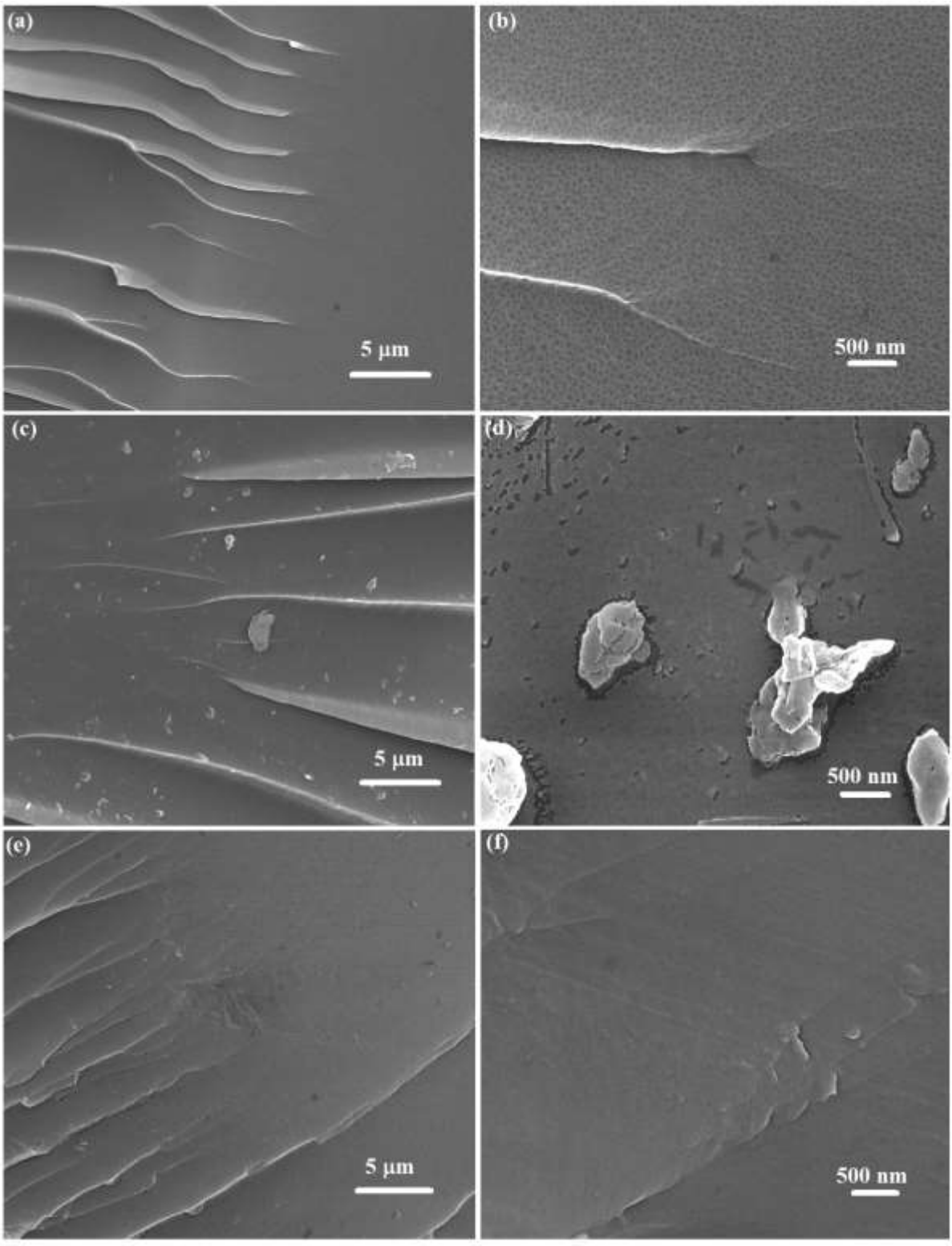

Figure 8 - Fracture surface micrograph of (a-b) neat epoxy, (c-d) GO/epoxy and (e-f) AGO/epoxy.

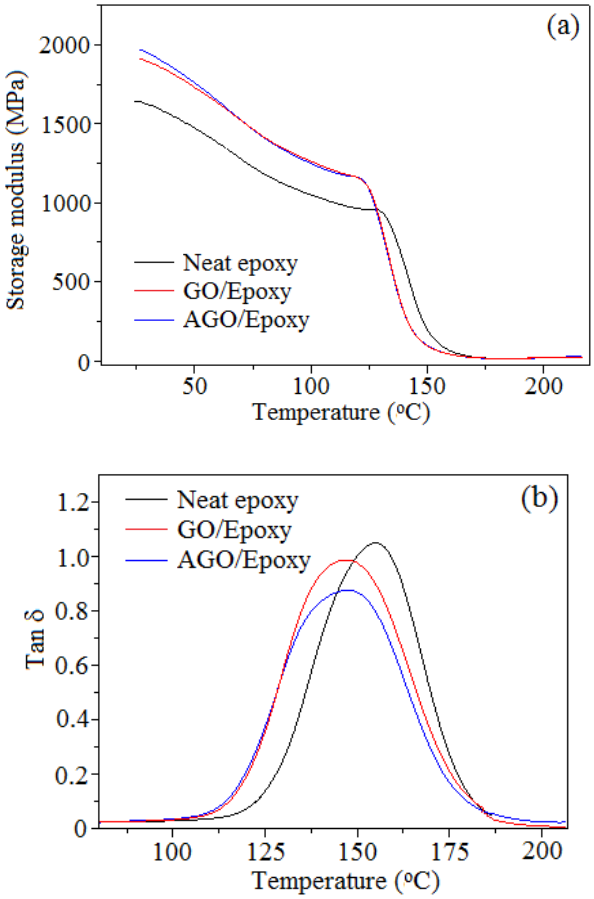

Figure 9 - (a) Storage modulus and (b) tan δ of neat epoxy and composites containing 1 wt.% of GO and AGO.

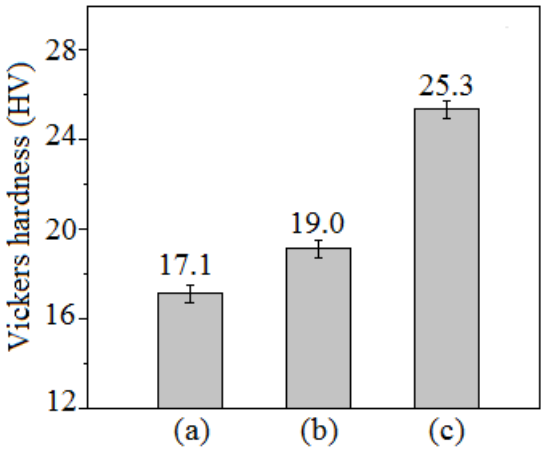

Figure 10 - Vickers hardness of the samples (a) neat epoxy, (b) GO/epoxy and (c) AGO/epoxy.

Tables

Table 1. Assignments of the FT-IR peaks

Sample	Peak (cm^{-1})	Interpretation	References
Graphite	3400	ν OH	[22]
	2924	ν_a CH_2	[23,24]
	2861	ν_s CH_2	[23,24]
	1639	ν C=C	[25,26]
GO	3400	ν OH	[22]
	1730	ν C=O	[27,28]
	1222	ν C-O	[29,30]
	1049	ν C-O	[29,30]
AGO	3425	ν NH_2	[31]
	1570	ν N-H	[29]

1116	ν C-N	[29]

ν = stretching vibrations; ν_a = asymmetric stretching vibrations; ν_s = symmetric stretching vibrations

Table 2 - Comparison of atomic compositions of GO and AGO determined by C1s XPS deconvolution.

Chemical bond	GO	AGO
C=C, C-H	46.6	35.6
C-O, C=O, O-C=O	53.4	38.5
C-N	-	25.9

Table 3 - Storage modulus, peak height of tan δ curve and Tg from DMA of samples.

Sample	E´ at 30 ^{o}C (MPa)	Peak height of tan δ curve	T_g (^{o}C) from curve tan δ
Neat resin	1553.1	1.05	164.8
GO/Epoxy	1892.8	0.98	157.1
AGO/Epoxy	1948.5	0.87	157.5